Journal of Quantitative Spectroscopy & Radiative Transfer 202 (2017) 200–209

Contents lists available at ScienceDirect

Journal of Quantitative Spectroscopy & Radiative Transfer

journal homepage: www.elsevier.com/locate/jqsrt

# Analysis of IR-bright regions of Jupiter in JIRAM-Juno data: Methods and validation of algorithms

D. Grassi[a,*], N.I. Ignatiev[b], G. Sindoni[a], E. d'Aversa[a], T. Maestri[c], A. Adriani[a], A. Mura[a], G. Filacchione[a], B.M. Dinelli[d], R. Noschese[a], A. Cicchetti[a], G. Piccioni[a], D. Turrini[a,e], F. Tosi[a], M.L. Moriconi[f], A. Olivieri[g], C. Plainaki[g], M. Amoroso[g], S.K. Atreya[h], G.S. Orton[i], S. Bolton[j]

[a] *Istituto di Astrofisica e Planetologia Spaziali – Istituto Nazionale di Astrofisica, Rome, Italy*
[b] *Institute of Cosmic Research, Russian Academy of Sciences, Moscow, Russia*
[c] *Dipartimento di Fisica e Astronomia, University of Bologna, Italy*
[d] *Istituto di Scienze Atmosferiche e del Clima, Consiglio Nazionale delle Ricerche, Sede di Bologna, Italy*
[e] *Departamento de Fisica, Universidad de Atacama, Copiapò, Chile*
[f] *Istituto di Scienze Atmosferiche e del Clima, Consiglio Nazionale delle Ricerche, Sede di Roma, Italy*
[g] *Agenzia Spaziale Italiana, Sede di Matera, Italy*
[h] *Department of Climate and Space Sciences and Engineering, University of Michigan, Ann Arbor, Michigan, USA*
[i] *Jet Propulsion Laboratory, California Institute of Technology, Pasadena, CA, USA*
[j] *Southwest Research Institute, San Antonio, Texas, USA*

ARTICLE INFO

*Article history:*
Received 13 April 2017
Revised 8 August 2017
Accepted 9 August 2017
Available online 10 August 2017

ABSTRACT

In this paper, we detail the retrieval methods developed for the analysis of the spectral data from the JIRAM experiment on board of the Juno NASA mission [1], operating in orbit around Jupiter since July 2016. Our focus is on the analysis of the thermal radiation in the 5 μm transparency window in regions of lesser cloud opacity (namely, hot-spots).

Moving from the preliminary analysis presented in [2], a retrieval scheme has been developed and implemented as a complete end-to-end processing software. Performances in terms of fit quality and retrieval errors are discussed from tests on simulated spectra, while some example and issue from usage on actual Jupiter data are also discussed.

Following the suggestion originally presented in [3] for the analysis of the data from the Near Infrared Mapping Spectrometer (NIMS) on board of the NASA Galileo spacecraft, the state vector to be retrieved has been drastically simplified on physically sounding basis, aiming mostly to distinguish between the 'deep' content of minor gaseous components ($H_2O$, $NH_3$, $PH_3$) and their relative humidity or fractional scale height in the upper troposphere. The retrieval code is based on a Bayesian scheme [4], complemented by simulated annealing method for most problematic cases.

The key parameters retrievable from JIRAM individual spectra are the $NH_3$ and $PH_3$ deep contents, the $H_2O$ vapor relative humidity as well as the total aerosol opacity.

Limitations related to the approximations of forward model methods are also assessed quantitatively.


## 1. Introduction

The Jupiter InfraRed Auroral Mapper (JIRAM) is an instrument on board of the NASA Juno spacecraft [1,5]. JIRAM includes a slit spectro-imager, operating in the near infrared spectral region (2–5 μm) and two image channels. The M filter channel acquires images in a broad spectral range centered around 5 μm, while the L channel passband is centered around 3.3 μm. The M and L channels are intended to provide the spatial context of the spectral data during the observations of the thermal emissions from the upper troposphere (down to approximately 6 bar for cloud-free conditions, but usually limited to the altitude of upper cloud deck between 1 and 0.7 bar) and the aurorae, respectively. Adriani et al. [1] discussed extensively the science objectives of the JIRAM experiment. Among them, the studies of the composition of the upper troposphere and of the properties of the auroral emissions are the ones that have driven both the design of the instrument and the observations planning.

This work describes the main properties and performances of a retrieval code developed for the analysis of JIRAM spectra in the

* Corresponding author.
*E-mail address:* davide.grassi@iaps.inaf.it (D. Grassi).

http://dx.doi.org/10.1016/j.jqsrt.2017.08.008
0022-4073/

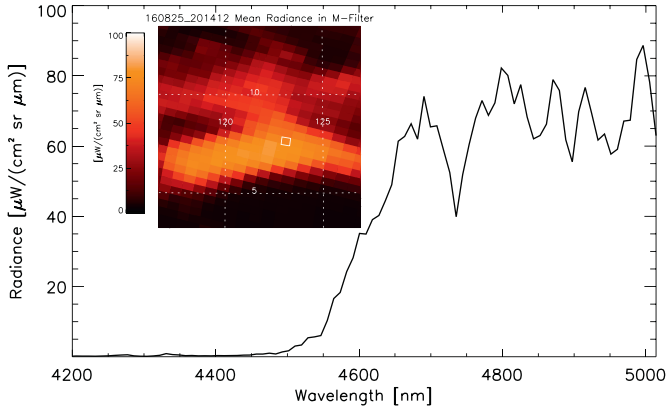


**Fig. 1.** Example of a JIRAM spectrum acquired in the brightest parts of a Jupiter Hot Spot (198th spectrum from frame JIR_SPE_RDR_2016238T205131_V01.DAT). The inset box map shows the spectrometer pixel borders. Spatial resolution is approximatively 500 km and emission angle is 29.5°. The spectrum was acquired at 7.8 local solar time (sun-zenith angle of 64°).

5 μm methane transparency window to obtain information on the composition of the upper troposphere. In fact, this spectral region is particularly interesting because it hosts the spectral lines of several minor constituents of Jupiter atmosphere like $H_2O$ and $NH_3$, that are the main carriers of oxygen and nitrogen in Jupiter atmosphere. Moreover, the 5 μm region is spectrally far enough from the peak of the solar radiation and therefore it is largely dominated by the thermal emission of the atmosphere. Fig. 1 shows an example of the JIRAM spectrum acquired over an Hot Spot in this spectral region at 7.8 local solar time (sun-zenith angle of 64°).

Jupiter emission at 5 μm has been observed at low and intermediate latitudes with space- and ground-based observations (see [6], for a recent example). Few bright distinctive areas were noted: the Hot Spots (the brightest features), associated with the grey 'festoons' observed in the optical domain between the Equatorial zone and the North equatorial Belt [7]; the rim of the Great Red Spot; the entire South Equatorial Zone and the areas surrounding the white ovals in the South-South Tropical Belt. In the bright areas, the thermal photons emitted at an effective level of a few bars are marginally absorbed by the clouds, allowing to probe the deeper parts of the troposphere. The ultimate source of opacity at 5 μm is represented by the molecular hydrogen collision-induced absorption, which - even in the absence of other minor components or clouds – reaches an optical thickness of 1 around the 5.5 bars level.

Nonetheless, most of the Jupiter's disk appears dark at 5 μm, suggesting a full coverage by thick clouds: indeed thermochemical equilibrium models for globally averaged conditions of Jupiter [8,9] predict three cloud levels of different compositions - extended over several tens of kilometers in altitude – derived from the condensation of $H_2O$, $NH_3$ and $NH_4SH$. The brightness temperature study by Drossart et al. [10] demonstrated that, at least in the equatorial region, the uppermost level of putative $NH_3$ ice must have some residual transparency, allowing some radiation from the warmer regions below to escape to space. Further analysis by Irwin et al. [11] found that brightness changes at 5 μm are mostly correlated with opacity changes of cloud layers lying at pressure levels between 1 and 2 bars than to variability of the higher $NH_3$ clouds. In accordance with models, these layers are expected to be composed mostly by $NH_4SH$, but the lack of detection of expected spectroscopic signature suggests that a substantial fraction of other materials must also be present.

## 2. JIRAM data

The JIRAM spectrometer covers the 2–5 μm range with a sampling step of about 10 nm and a nominal spectral resolution of about 12 nm. The JIRAM spectra are acquired simultaneously along a slit of 256 spatially-adjacent pixels. The field of view of individual pixels (in the spectrometer as well as in the imager) is 250 μrad.

Spatial resolution at the nominal 1-bar level varies greatly because of the large eccentricity of Juno's orbit. Albeit JIRAM data are collected in the vicinity of pericenter, strong variations of the Juno-Jupiter distance are found in the dataset. For example, during the first perijove of August 2016, more than $1.1 \cdot 10^6$ JIRAM spectra were acquired at distances ranging from $2.5 \cdot 10^6$ to $8.6 \cdot 10^4$ km, with corresponding fields of view between 625 and 21 km. The mean distance in the same period was $1.04 \cdot 10^6$ km, corresponding to a spectral field of view of 250 km.

Juno is a spinning spacecraft, and by design, JIRAM slit is parallel to the spin axis in order to allow rotation compensation during the exposure with typical duration of 1 s for the spectrometer.

Data acquired during the flyby of the Moon in October 2013 [5] and during the first perijove [12] demonstrated that JIRAM spectrometer benefits from excellent radiometric performances. A preliminary estimate performed prior to Jupiter orbit insertion set the Noise Equivalent Radiance (NER) value at 5 μm around $1.8 \times 10^{-1}$ μW/(cm$^2$ sr μm). This value was adopted in the analysis described below.

## 3. Description of the retrieval code

The information content of individual JIRAM spectra has been described in the preparatory work of [2]. Starting from these concepts, we developed an end-to-end retrieval code based on the Bayesian formalism [4]. The code is largely derived from a similar software previously developed for the analysis of VIRTIS-Venus Express data [13]. The code is intended to study the composition of the upper troposphere – between the 6 and 1 bar levels – at locations where a moderate cloud optical thickness ($\tau < 1$) allows the thermal radiation to be emitted in the considered pressure range for measurements from space. Hot Spots were considered as study cases during development.

Despite the advances in computer speeds and storages from the NIMS era, computational time remains a major issue for a code aimed to process a very large dataset such as the one expected from JIRAM (in the order of $10^7$ spectra). The analysis of each spectrum requires typically twenty iterations, and a minimum of 15 forward simulations (computation of the expected spectrum for given physical conditions of the atmosphere) are required at each iteration. Even with pre-computed tables of gaseous opacity available, line-by-line radiative transfer simulation of a single spectrum according the DISORT algorithm [14] requires a time in the order of 40 s on the test computer used for the code development (Intel Core i7 2.8 GHz, 4GB RAM). In these conditions, we deemed necessary to adopt simplified, albeit approximate, methods for the treatment of forward radiative transfer. The current version of the code (February 2017) includes a forward radiative transfer model based on the correlated-k method [15] considering 30 quadrature points. The correlated-k method has been adopted for the sole purpose to reduce drastically the number of points where radiative transfer computation shall actually be performed. Historically, another advantage of the correlated-k method has been the possibility to derive correlated-k coefficients for different gases directly from moderate resolution experimental measurements [16]. However, the degree of completeness achieved by line parameters lists such as HITRAN [17] in the spectral region of our interest ($\lambda > 2$ μm) has made this advantage not relevant for our purposes.

Radiative transfer equation at each quadrature point is solved according the two-streams approximation, as implemented in [18] by Eqs. (1)–(8) and (19)–(43) therein. The joint usage of correlated-k and two-streams approximations allowed a reduction of the time required by the radiative transfer simulation of a single spectrum to 1.2 s.

The retrieval code considers the spectral range between 4 and 5 μm and only the thermal source. While of obvious interest, the inclusion of the solar-dominated spectral range of 2–4 μm would require the treatment of solar scattering, with significant computational burden and considerable uncertainties in the forward modeling errors related to the assumptions on the cloud properties (this is especially true for the upper cloud deck and haze). On the other hand, the 'no solar source' approximation is partly justified by our specific focus on the more transparent regions, assumed to correspond to the brightest areas where the analysis of [10], found that the scattered solar contribution is between 100 and 800 times smaller than the thermal component.

The atmosphere is modeled as a stack of 43 plane-parallel levels, uniformly spaced in log(p) between 22 bar and 38 millibar. The vertical temperature profile is fixed and assumed to be the one measured by the Galileo Entry Probe [19].

The code takes into account the opacities of $CH_4$, $H_2O$, $NH_3$, $PH_3$, $AsH_3$, $GeH_4$ and $H_2$ absorption induced by collisions (CIA) with $H_2$ itself, He and $CH_4$. The treatment of the far wing shapes and line cut-offs values as long as the spectroscopic data for these gases are similar to those reported in [2]. A few differences should be noted: data derived from HITRAN were updated to the latest HITRAN 2012 release [17], the line-mixing effects for the strongest lines of $\nu_3$ $CH_4$ band were included according to the method described in [20], $PH_3$ line parameters were integrated with the publicly-available section of the data described in [21,22]. Line-by-line computation of the opacities of gases at different temperatures and pressures are eventually used to create a file of correlated-k coefficients for each gas. These coefficients files needs to be computed only once and can be used for the any subsequent simulation including the gas of interest.

Following Giles et al. [23], we adopted a very simple model for the putative $NH_4SH$ cloud, assumed to have a single scattering albedo $\omega = 0.9$ and an Henyey–Greenstein phase function corresponding to an asymmetry factor $g = 0.7$ in the entire spectral range of interest. The single scattering albedo and the asymmetry factor are used in Eqs. (3)–(6) of [18] to handle the anisotropic scattering of particles. The cloud is assumed to lie between the 0.75 and 1.3 bar levels, values roughly consistent with the GEP nephelometer data [24]. This is the only cloud included in our retrieval scheme. This assumption is indeed rather strong, since it has been derived from the very specific conditions (extreme dryness, very low opacity) experienced by the GEP. In matter of fact, care shall be exercised in interpreting results for opacities at 5 μm greater than an approximative value of 1, since these could likely correspond to more complex cloud structures. Namely, with increasing optical thickness, clouds are expected to become more extended in altitude (with a non negligible gradient of opacity along air temperature) and to show considerable opacities well below the 2 bar level [9].

Following the approach presented in [3], we considered a rather simple set of free atmospheric parameters to model the observed spectra. The vertical mixing ratios of $H_2O$ and $NH_3$ are described by two free parameters each: an altitude-independent relative humidity (RH), for altitudes above the condensation level and a uniform deep mixing ratio for altitudes below the condensation level. $PH_3$ vertical mixing ratio is considered to be uniform below the 1 bar level, while above this level it decreases with increasing altitude according to a fixed relative fraction of the local scale height (FSH). $AsH_3$ and $GeH_4$ mixing ratios are allowed to vary, but are assumed to be uniform with altitude. The last free parameter is the total opacity of the 1-bar cloud. Fig. 2 summarizes the free parameters of the retrieval code.

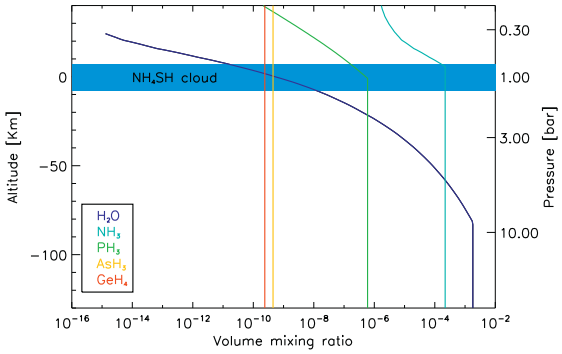


**Fig. 2.** Simplified gaseous mixing ratio profiles assumed as free parameters to fit observed spectra.

The retrieval of the above mentioned parameters is performed using an iterative Gauss–Newton procedure, inclusive of a Levenberg–Marquardt method ([4], Eq. (5.36)), required to avoid convergence to local minima. The iterations stop when the changes of the retrieved parameters between consecutive iterations are within the formal retrieval errors. More precisely, we adopted the $d_i^2$ criterion given by expression (5.29) in [4]. A final evaluation is performed comparing the residuals and JIRAM NER: a simulated annealing method (as presented by Press et al. [25]) is eventually invoked if the value of $\chi^2$ (defined for this purpose as the mean quadratic difference between the best-fit and observed spectrum as weighted by the NER) exceeds a given threshold level.

We choose to retrieve the logarithm of the free parameters (i.e.: the elements of the state vector) to avoid non-physical negative values. The a priori values of the state vector, as well as the corresponding standard deviations used to build up the uncorrelated a priori covariance matrix $S_a$ are taken from [3] and are listed in Table 1. Note that the tests described in Section 4 demonstrated the actual insensitivity of our data to the $NH_3$ relative humidity and $PH_3$ relative scale height: consistently, these parameters are not reported in Table 1. During retrieval they are set to 13% and 25%, respectively. Off-diagonal elements of $S_a$ are set to zero.

## 4. Validation

Our analysis tools have been preliminary validated on simulated observations, prior to the orbit insertion of Juno. These activities, described in this Section 4, were performed by removing from atmospheric composition $GeH_4$, $AsH_3$ and CO, whose spectral effects, were deemed as minor compared to the spectral signatures of $CH_4$, $H_2O$, $NH_3$ and $PH_3$, as discussed in [2]. The validation tests described in this section were performed assuming an observation emission angle of 25°, to be compared against a mean value of observation emission angle of JIRAM spectra acquired during the first perijove of 32°

### 4.1. Forward model approximations

The errors introduced by the approximations made in the development of the forward model have been estimated statistically with numerical tests. First, we created a population of different input state vectors. Then, for each state vector, we computed the simulated spectrum with a) the algorithm embedded in the retrieval code with b) a *much* slower full physics line-by-line code. In the latter case we used a much finer vertical discretization (171 levels) and the scattering was accounted for with the DISORT al-

**Table 1**
Retrieved parameters: $x_a$ is the a priori value of the parameter, while the $10^{xa}$ elements give the equivalent, commonly-used, physical quantities (ppv stands for parts per volume, i.e. molar fraction). $\sigma(x_a)$ is the corresponding standard deviation used to build the $S_a$ covariance matrix, and $\sigma(x)$ is the square root of the covariance matrix $S$ of the retrieval, as computed at the first iteration.

| | $[H_2O]_{deep}$ | $[H_2O]_{RH}$ | $[NH_3]_{deep}$ | $[PH_3]_{deep}$ | $[AsH_3]_{deep}$ | $[GeH_4]_{deep}$ | $\tau$ @ 5μ |
|---|---|---|---|---|---|---|---|
| $x_a$ | −2.74 | 1.00 | −3.66 | −6.22 | −9.34 | −9.62 | 0. |
| $10^{xa}$ | $1.81\times10^{-3}$ [ppv] | 10. [%] | $2.2\times10^{-4}$ [ppv] | $6.\times10^{-7}$ [ppv] | $4.5\times10^{-10}$ [ppv] | $2.4\times10^{-10}$ [ppv] | 1. |
| $\sigma(x_a)$ | 1.0 | 0.48 | 0.56 | 0.63 | 0.5 | 0.5 | 1. |
| $\sigma(x)$ | 0.884 | 0.012 | 0.012 | 0.006 | – | – | 0.005 |

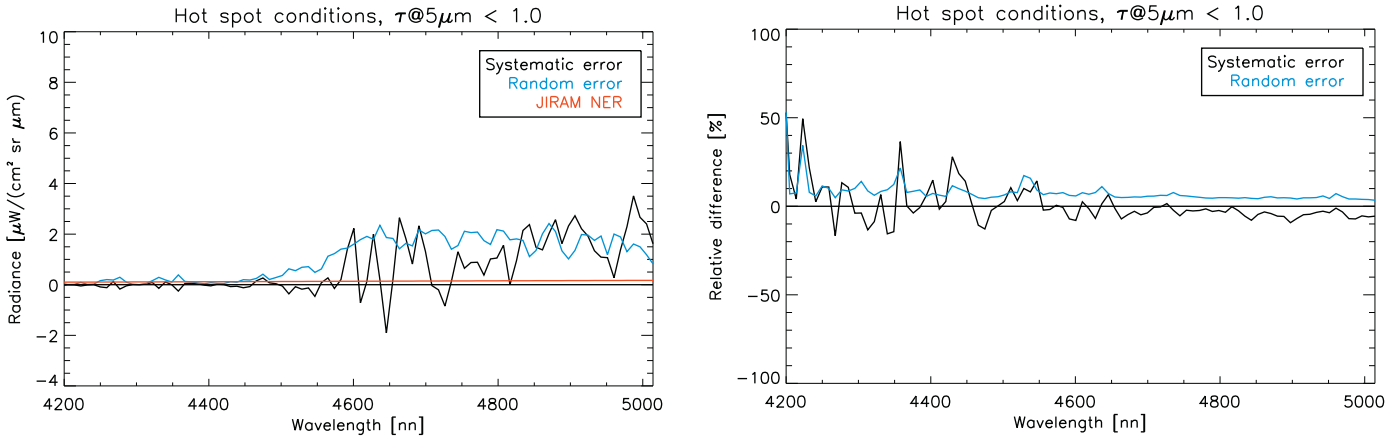


**Fig. 3.** Performances of the forward radiative transfer model embedded in the retrieval code, as assessed against the results obtained using a full line-by-line code based on DISORT and with a high density vertical sampling. Panel a.: systematic and random components of differences, in absolute terms. Panel b.: systematic and random components of differences, in relative terms with respect to line-by-line code.

gorithm [14], after the expansion of the Heyney–Greenstein phase function (with g = 0.7) in Legendre polynomials. Statistical comparison of spectra against their counterparts allows a quantitative assessment of the impact of the forward model approximations. Parameters included in the state vector are: $[H_2O]_{deep}$, $[H_2O]_{RH}$, $[NH_3]_{deep}$, $[NH_3]_{RH}$, $[PH_3]_{deep}$, $[PH_3]_{FSH}$ and cloud opacity at 5 μm. The population of the input state vectors was created as follows. For each element of the population:

1. We created a set of 7 (statistically independent) random numbers with zero mean and standard deviation of 1.
2. The $\sigma(x_a)$ was multiplied by these random numbers and added to the $x_a$ elements listed in Table 1. For $\log_{10}([NH_3]_{RH})$ we assumed $x_a$ equal to 1.1 and $\sigma(x_a)$ equal to 0.477. For $\log_{10}([PH_3]_{FSH})$ we assumed $x_a$ equal to 1.39 and $\sigma(x_a)$ equal to 0.442. This returned a random state vector.

The test was repeated for 256 cases (total size of the test population), the size being justified by the aim to reproduce a JIRAM slit. The JIRAM slit has a length of 256 pixels, and JIRAM acquires simultaneously the spectrum for each of the 256 pixels. In order to simulate extended spatial features as seen over the Jupiter disk, the values corresponding to the same physical parameter *in different cases* (different spectra) are not statistically independent. In matter of fact, for each element of the state vector, we created a random array of length 256, where a correlation length of 35 was imposed along the array. This correlation length was achieved multiplying an initial array of length 256 of fully-independent random draws by the Cholesky decomposition of the required correlation matrix C. The correlation matrix C (of size $256 \times 256$) was defined as C[*i*,*j*]=exp(−((*i*−*j*)^2)/(L^2)) where *i* and *j* indexes vary from 1 to 256 and L is equal to 35.

Since we are interested mostly in the IR bright areas, the spectra comparison was limited to cases where the residual opacity of the 1-bar cloud was less than 1: this reduced the effective population size to 143. Fig 3a and b show the results in relative as well as absolute terms. Albeit the performances of the forward model are – at least in the spectral regions with high signal - in line with those expected for the correlated-k methods (better than 5% for the NEMESIS code [15]), they remain inadequate to fully exploit the excellent radiometric performances of JIRAM. At worst, the ratio between random modeling error and NER reaches values up to 15. Further tests – performed introducing the modeling approximations one by one and considering the mean amplitude of induced errors - demonstrated that the random modeling errors are mostly caused by the treatment of the scattering (consistently, they tend to diminish with decreasing residual opacity), secondly to the usage of correlated-k method instead of a full line-by-line approach and only marginally to coarser vertical sampling grid. The order is reversed for the systematic components. Despite the obvious limitations described above, no viable alternative is presently available for the forward modeling, since both the usage of DISORT or the adoption of a line-by-line code would increase the retrieval time from a few minutes to a few hours. Net effects of this compromise are described in the following section.

### 4.2. Retrieval performances

Validation of the retrieval code consists essentially in a direct estimate of the retrieval errors from numerical tests. Errors may arise from several factors:

1. Discrepancies between observed and best-fit spectrum. In the ideal case, this difference would show random fluctuations with a standard deviation equal to NER.
2. Approximations in the forward radiative transfer model, computing time driven (namely: correlated-k instead of line-by-line and two-streams instead of DISORT).
3. Uncertainties in the adopted parameterization of the vertical distribution of the gases.

4. Uncertainties in the spectroscopic aerosol and gas models (aerosol phase functions, spectroscopic line databases, far wing shapes, etc.).

The Bayesan approach directly maps the NER into the retrieval error, therefore point 1 of the above list is formally accounted for (see formula 5.13 in [4]). However, even in the ideal case, significant departures from ideal performances can be induced by the highly non-linear nature of the problem. In order to evaluate these effects, we performed a set of simulated retrievals. We considered the set of simulated observations performed with the forward model embedded in the retrieval code, with the parameters described in Section 4.1. We added a random error, with statistical properties equal to JIRAM NER, to the simulated spectrum. Then the simulated noisy spectrum was fed into the retrieval code and the results were compared with the state vector used into the simulation.

Fig. 4 shows the results limited to the cases where the residual cloud opacity is smaller than 1. Fig. 5 summarizes the modeling capabilities.

The retrieval code has demonstrated to behave nearly ideally: the final $\chi^2$ approaches 1 and the mean values of retrieval errors are close to the square root of the diagonal elements of the covariance matrix of the solution, as listed in the last row - $\sigma(x)$ - of Table 1. The relative humidity of $NH_3$ and $PH_3$ scale height were essentially not constrained, demonstrating the effective lack of information content in JIRAM data on these two parameters. This is not surprising, since both parameters describe the vertical profile of these gases at pressure levels not probed by JIRAM weighting functions (as shown in Fig. 2 of [2]). Deep mixing ratio of $H_2O$ is an ambiguous free parameter: given our parameterization of $[H_2O]$ vs. altitude, only *low* values of $[H_2O]_{deep}$ (approximatively $5\times10^{-4}$ ppv) determine a condensation level high enough in altitude to place the region of constant mixing ration within the pressure range probed by JIRAM. Conversely, in our simplified model, a constant deep mixing ratio of $H_2O$ is usually achieved well below the region probed by JIRAM weighting functions.

Similar runs on simulations at different emission angles confirmed that the code performances remain the same between the emission angles of 0° and 50°.

In order to assess the effects of the forward model approximations on the retrievals the same test was repeated analyzing the spectra simulated with the full physics code (line-by-line, DISORT, 171 levels). The emission angle was set again to 25°. Figs 6 and 7 summarize the retrieval performances. Noteworthy, in this further run the retrieval code still retained in its forward radiative transfer subroutine the correlated-k and two-streams approximations. The retrieval code is capable to model the observed spectra with an accuracy better than the typical errors associated to the forward model approximations (compare Figs. 3a and 7b): some systematic retrieval errors due to over-fit (i.e.: the effort of the algorithm to match the data at the level of formal NER despite actual greater forward modeling uncertainties) of data are therefore to be expected. Albeit the radiative transfer approximations reduce the overall performances, the code retains its capability to reduce substantially the uncertainty with respect to the realistic variations used to define the a priori variance. Table 2 summarizes retrieval performances as inferred from these two numerical tests. The parameter most adversely affected by forward model approximations is probably the total opacity: the slight systematic excess in the estimate of radiance for a given state vector are erroneously compensated during the retrieval increasing the retrieved values of the opacity. This effect is particularly evident for very low opacity values.

The same numerical approach is less effective for factors 3 and 4. Here, we are not dealing with deliberate simplifications, but with alternative hypothesis to our best-guess assumptions. Therefore, the guesses required to create populations of simulated spectra would become more and more questionable. For practical purposes, the last two rows of Table 2 provides an effective *minimal* estimate of retrieval errors from JIRAM data with the current code.

## 5. Use on real JIRAM data

The arrival of the Juno spacecraft at Jupiter allowed the first assessment of the actual instrument performances, namely:

- Standard deviation of the calibrated JIRAM observations of the deep space, as acquired pointing far away from Jupiter disk, allow to estimate the component of the random error not associated to the signal photon noise in the actual operative thermal conditions. This component includes – among the others – the readout noise and the photon noise associated to the instrument thermal background (whose mean value is removed during the calibration process). The value of this component turns out to vary between 1.5 and $5\times10^{-2}$ μW/(cm$^2$ sr μm). On the other hand, photon noise related to Jupiter signal inside the 5 μm transparency window has a similar magnitude: i.e.: maximum of $2\times10^{-2}$ μW/(cm$^2$ sr μm). This latter component can be estimated from typical values of the square root of the number of photons from Jupiter collected by JIRAM in operative conditions and from the JIRAM radiometric responsivity (defined as the ratio between calibrated and raw spectra). The quadratic sum of these figures provides a rough estimate of the effective NER of JIRAM spectra and demonstrates that over bright hot spots a signal-to-noise ratio exceeding 500 is commonly achieved.
- Spectra of IR bright regions allow to validate the spectral calibration. We performed firstly a preliminary retrieval of atmospheric parameters from an actual JIRAM spectrum of a bright Hot Spot, assuming for the instrument the design spectral sampling grid and spectral resolution. From the retrieval results, we computed the expected theoretical spectrum at very high spectral resolution (0.01 cm−1). On this high resolution spectrum, we applied a series of convolutions to simulate JIRAM responses with different shifts on wavelength sampling grid and degradation factors for spectral resolution. On the basis of the best match with observed spectrum, we concluded that in the 5 μm transparency window the spectral sampling positions are essentially confirmed, while the effective spectral resolution is degraded by a factor of 1.3. Therefore, in this region the effective spectral resolution is about 16 nm.

Some further considerations arose from the retrieval code itself:

- It was immediately evident that $GeH_4$ and $AsH_3$ must be included in the atmospheric composition, in order to properly match the spectra.
- An attempt was made to introduce a deep (5 bar) cloud, following the approach presented by [26], but this methodology demonstrated to produce negligible improvements of the fit quality in the analysis of JIRAM Hot Spots spectra and therefore represented, in our opinion, an unnecessary complication. This option can still be included for the analysis of other regions, since [27] suggested that a similar structure may exists at latitudes different than those typical of the Hot Spot occurrence.

Fig. 8 shows two examples of retrievals using spectra extracted from the Hot Spot region of Fig. 1. In both cases, the average difference between observed and best fit spectrum are below 5%. Values of the atmospheric parameters retrieved in this region are discussed extensively in [28] and are essentially in line with previous expectations for Hot Spot conditions. Once the entire set of spectra

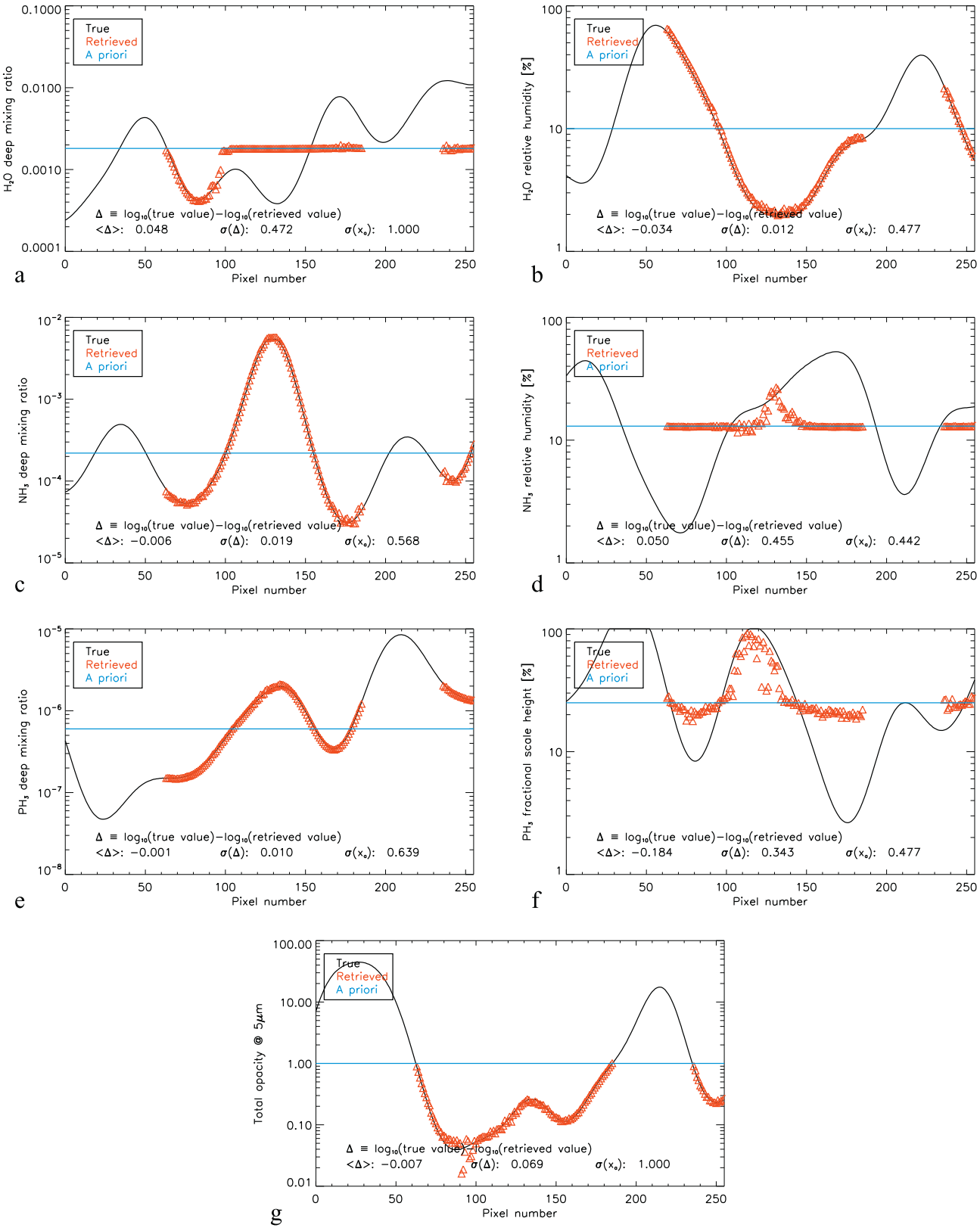


**Fig. 4.** Retrieval performances of analysis code, as estimated from a test run on a population of simulated observations. Each panel compares the input values (black curves) used to compute the simulated spectra against the retrieved values (red triangles). Each triangle corresponds to an individual spectrum, independently analysed. Comparison is performed only for cases where residual opacity of 1-bar cloud is less than 1. Each panel reports also: $\langle\Delta\rangle$, the mean difference between true and retrieved value; $\sigma(\Delta)$, the standard deviation of the difference between true and retrieved value; $\sigma$(xa), the standard deviation of the corresponding element in the a priori state vector. Panel a: log10 of deep $H_2O$ vapor mixing ratio; Panel b: $\log_{10}$ of $H_2O$ vapor relative humidity; Panel c: log10 of deep $NH_3$ mixing ratio; Panel d: $\log_{10}$ of $NH_3$ relative humidity; Panel e: $\log_{10}$ of deep $PH_3$ mixing ratio; Panel f: $\log_{10}$ of $PH_3$ relative scale height; Panel g: $\log_{10}$ of 5 μm opacity of the residual 1-bar cloud. (For interpretation of the references to color in this figure legend, the reader is referred to the web version of this article.)

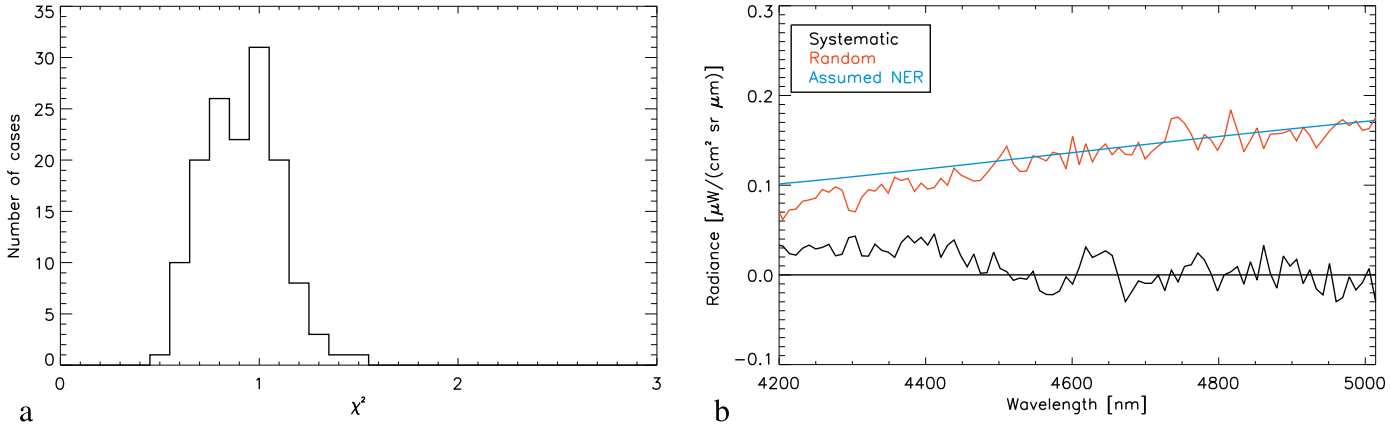


**Fig. 5.** Modeling performances of analysis code, as estimated from a test run on a population of simulated observations. For both panels, only cases where residual opacity of 1-bar cloud is less than 1 were considered. Panel a: distribution of $\chi^2$ for fit residuals. Panel b: differences between observed (simulated) data and best-fit spectra. Black curve ("systematic"): mean difference, as computed over the population; red curve ("random"): standard deviation of the difference; blue curve: NER value assumed for the test. (For interpretation of the references to color in this figure legend, the reader is referred to the web version of this article.)

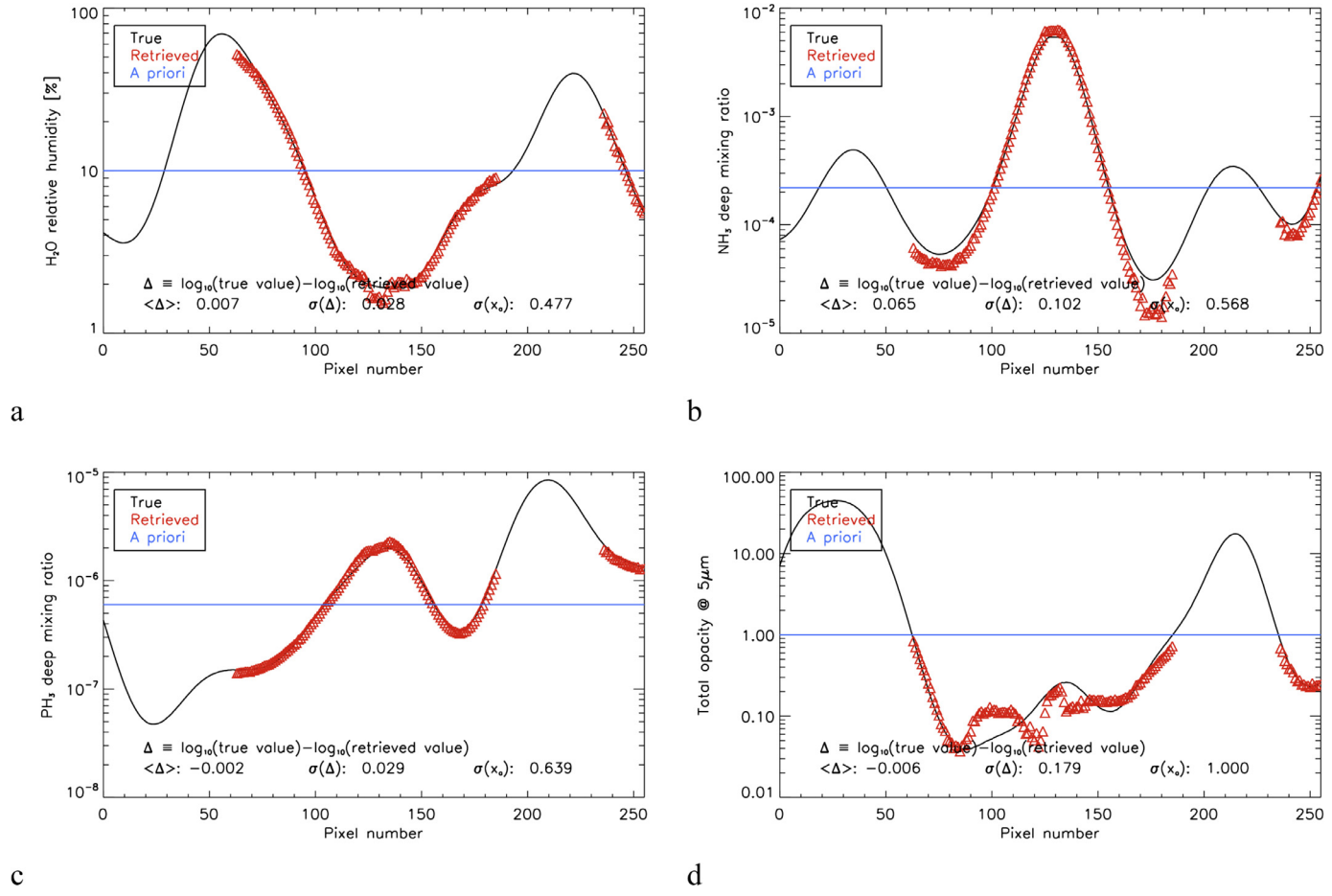


**Fig. 6.** The same as Fig. 4, but applying the analysis code to a population of simulated spectra computed using a full line-by-line code inclusive of DISORT. This test provides our current best simulation of actual operative conditions.

with a retrieved cloud opacity lesser than 1 is taken into account (for a total of 107 spectra) and the corresponding population of the spectral fit residuals is considered, some systematic differences (Fig. 9) can be noted:

- The depth of the strong minimum at 4.95–4.96 μm is seldom reproduced in the simulated spectra. This feature is associated to the $H_2O$ vapor absorption and cannot be improved including in the forward model the MT_CKD continuum [29]. Albeit similar models for $H_2O$ vapor continuum were used in past analyses of the Jupiter atmosphere [3], their use remains questionable, since they have been empirically derived for Earth-like condi-

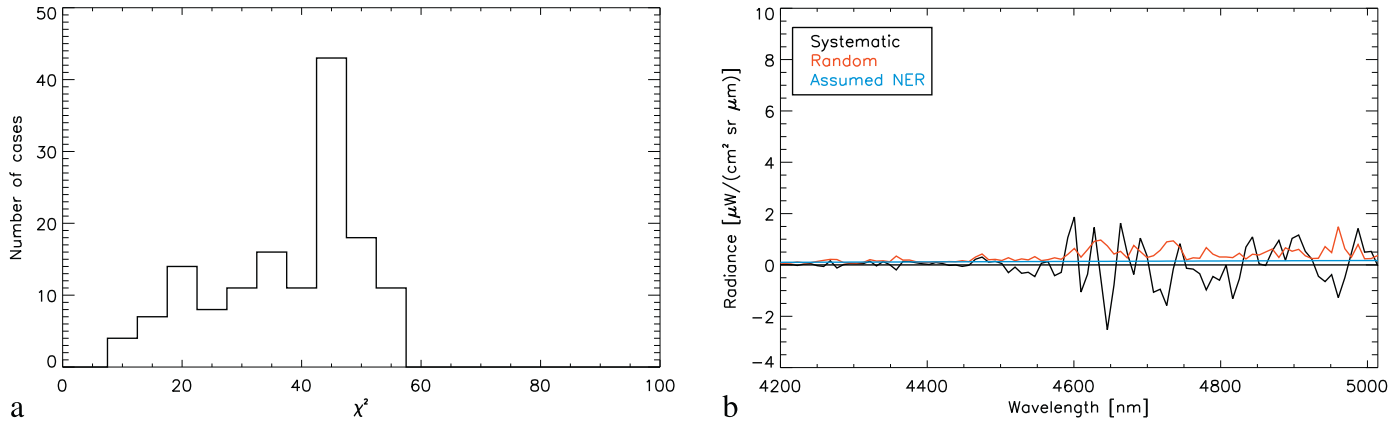


**Fig. 7.** The same of Fig. 5, but applying the analysis code (that still retains in its forward radiative transfer subroutine the correlated-k and two-streams approximations) to a population of simulated spectra computed using a full line-by-line code inclusive of DISORT. The degradation of performances with respect to Fig. 5 represents the net effect of the limits in the treatment of forward radiative transfer.

**Table 2**
Retrieval performances of the analysis code, as inferred from numerical tests. $\sigma$(xa) elements are the corresponding standard deviations used to build the Sa covariance matrix. $\sigma$(x) are the square roots of the diagonal elements of the solution covariance matrix S, as computed at the first iteration. $\langle\Delta\rangle$ is the mean difference between true and retrieved value; $\sigma(\Delta)$ is the standard deviation of the difference between true and retrieved value. "scrt" subscript (as for "self-consistent ratiative transfer treatment") refers to the test on simulated observations computed using the same radiative transfer code embedded in the analysis code, "irta" (as for "inclusive of radiative transfer approximations") subscript refers to the test on simulated observations computed using a full line-by-line code inclusive of DISORT but retaining the radiative transfer approximations (correlated-k and two-streams) in the retrieval code. The last two rows (corresponding to the "irta" case) represent our best estimate of retrieval errors from the current code, in their systematic and random components, respectively.

| | $Log_{10}([H_2O]_{deep})$ | $Log_{10}([H_2O]_{RH})$ | $Log_{10}([NH_3]_{deep})$ | $Log_{10}([PH_3]_{deep})$ | $Log_{10}(\tau$ @ 5μ) |
|---|---|---|---|---|---|
| $\sigma(x_a)$ | 1.0 | 0.48 | 0.57 | 0.63 | 1. |
| $\sigma(x)$ | 0.884 | 0.012 | 0.012 | 0.006 | 0.005 |
| $\langle\Delta\rangle_{scrt}$ | 0.048 | −0.034 | −0.006 | −0.001 | −0.007 |
| $\sigma(\Delta)_{scrt}$ | 0.472 | 0.012 | 0.019 | 0.010 | 0.069 |
| $\langle\Delta\rangle_{irta}$ | 0.122 | 0.007 | 0.065 | −0.002 | −0.006 |
| $\sigma(\Delta)_{irta}$ | 0.559 | 0.028 | 0.102 | 0.029 | 0.179 |

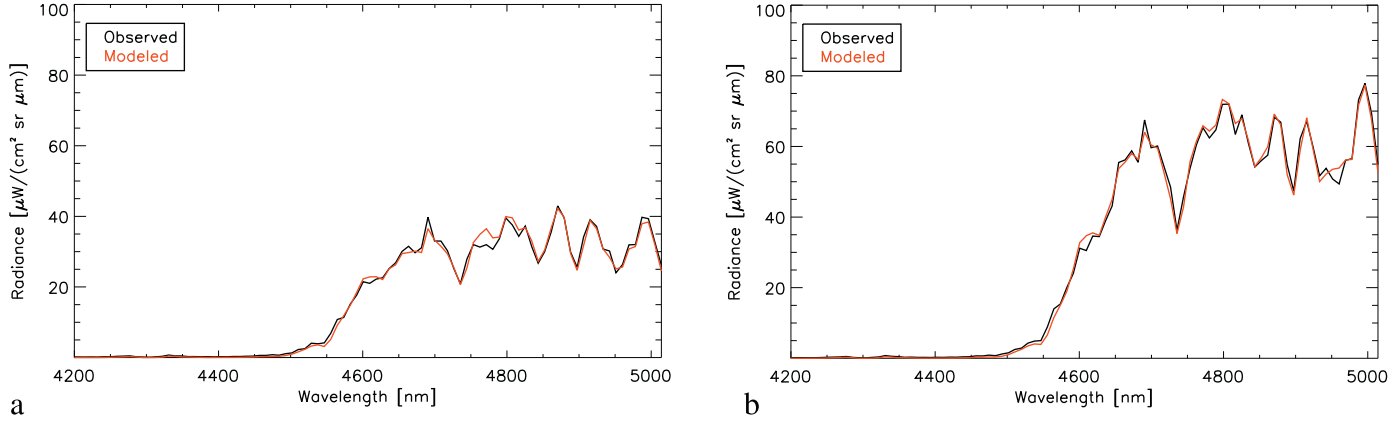


**Fig. 8.** Two examples of fitting of actual JIRAM data. Both examples are from the same Hot Spot presented in Fig. 1 and extensively discussed in [28].

tions and their extension to the Jupiter $H_2$-dominated environment can produce systematic errors.

- A similar behavior is observed for the minimum at 4.78 μm, associated to $H_2O$ vapor too.
- The minimum observed at 4.61 μm cannot be reproduced by our best fit spectra, as well as the inflection at 4.57 μm. In our forward model we considered a spectral resolution degradation factor equal to 1.3, constant over the entire spectral range. This value however is purely empirical, and one may suppose that a lesser degradation around 4.6 μm could partially mitigate these misfits. This hypothesis however is not supported by tests with different degradation factors, where no clear trend in the quality of the fit can be derived in this spectral range.
- The peak at 4.69 μm appears often smoother in the best-fit spectra than in the observed ones.

Noteworthy, the misfits observed while modeling real JIRAM data show magnitudes similar to those described in Fig. 3 and re-

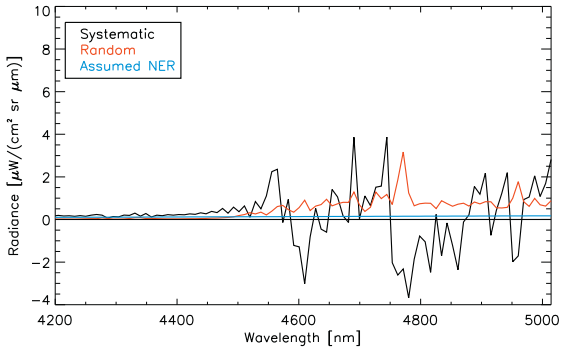


**Fig. 9.** Modeling performances of the analysis code once applied to actual JIRAM data, as estimated from the differences between observed data and best-fit spectra. Black curve ("systematic"): mean difference, as computed over the population; red curve ("random"): standard deviation of the difference; blue curve: NER value assumed for the test. Statistics were computed from the 107 spectra with a retrieved opacity <1 from Hot Spot #1 discussed in [28], the same presented in Fig. 1. (For interpretation of the references to color in this figure legend, the reader is referred to the web version of this article.)

lated to the forward model approximations. In particular, the region at 4.96 μm was one where the systematic and random components of the forward model errors is maximum. It is therefore reasonable to suspect that misfits presented in Fig. 9 are – at least partially – related to forward modeling approximations.

In these circumstances, the use of $\chi^2$ to quantify fit quality results too punitive (unless the forward model error is considered to compute an "effective" NER) and we opted to consider in future science analysis the relative percentage discrepancy between observed and best-fit spectrum (averaged over the 4.6–5 μm range) as the most pertinent fit-quality parameter.

## 6. Future work

The development of the analysis code presented here had as a major goal to provide the JIRAM team a robust tool ready for the preliminary analysis of the data at the time of the first Juno pericenter passage. Going forward, there are a number of potential improvements we plan to test in the future:

1. *Set of retrieved parameters* In [2], we demonstrated that - even with the NER levels expected at that times (about 100 times higher than actually observed) – JIRAM spectra have about 17 degrees of freedom for signal, a number much higher than the number of variables currently retrieved. On the basis of the kernels curves presented in Fig. 3 of [2], one can envisage as possible improvement the retrieval of the vertical profiles of $H_2O$ vapor (between 4 and 6.8 bars) and $NH_3$ (between 4 and 6 bars), as well as the vertical profile of $PH_3$ (in the rather large range between 1 and 6.8 bars).
2. *Forward methods* Tests on simulated observations demonstrated that the approximations in the forward model represent the main error source in our current analysis scheme. Among the improvements that can be made we can mention the replacement of the two-streams with the multiple-scattering matrix operator [30], also adopted in the well-established NEMESIS code [15]. More difficulty is to envisage the complete replacement of the correlated-k approach: a full line-by-line treatment added to the scattering evaluation at each point of the pseudo-monochromatic grid is computationally too expensive. A possible alternative, is represented by the so-called 'correlated-I' method discussed in [31], but remains be tested under Jovian conditions.

## Acknowledgments

This work was supported by the Italian Space Agency through ASI-INAF contract I/010/10/0 and 2014-050-R.0. JIL and SKA acknowledge support from NASA through the Juno Project. GSO acknowledges support from NASA through funds that were distributed to the Jet Propulsion Laboratory, California Institute of Technology (Grant NNN12AA01C).

H. Tran (Laboratoire Interuniversitaire des Systèmes Atmosphériques) kindly provided the code for line mixing of methane.

Development of the retrieval code greatly benefited of discussions with P. Irwin, L. Fletcher, R. Giles, T. Fouchet, P. Drossart, M. Roos-Serote and L. Kedziora-Chudczer.

The JIRAM instrument has been developed by Leonardo at the Officine Galileo - Campi Bisenzio site.

The JIRAM instrument was conceived and brought to reality by our late collaborator and Institute director Dr. Angioletta Coradini (1946–2011). The work described here largely derives from the heritage of the Planetary Fourier Spectrometer for Mars Express project, led by Dr. Vittorio Formisano (1941–2016) and the tools originally developed in IKI-RAS, Moscow, under the supervision of Prof. V. Moroz (1932–2004).

## References

[1] Adriani A, et al. JIRAM, the Jovian infrared Auroral mapper. Space Sci Rev 2014. doi:10.1007/s11214-014-0094-y.
[2] Grassi D, et al. Jupiter's hot spots: Quantitative assessment of the retrieval capabilities of future IR spectro-imagers. Planet Space Sci 2010;58:1265–78. doi:10.1016/j.pss.2010.05.003.
[3] Irwin PGJ, et al. Cloud structure and atmospheric composition of Jupiter retrieved from Galileo near-infrared mapping spectrometer real-time spectra. J Geophys Res 1998;103(E10):23001–21. doi:10.1029/98JE00948.
[4] Rodgers CR. Inverse methods for atmospheric sounding: theory and practice. Singapore: World Scientific; 2000.
[5] Adriani A, et al. Juno's Earth flyby: the Jovian infrared Auroral mapper preliminary results. Astrophys Space Sci 2016;361(8) article id.272.
[6] Fletcher LN, et al. Mid-infrared mapping of Jupiter's temperatures, aerosol opacity and chemical distributions with IRTF/TEXES. Icarus 2016;278:128–61. doi:10.1016/j.icarus.2016.06.008.
[7] Rogers JH. The giant planet Jupiter. Cambridge: University Press; 1995.
[8] Atreya SK, et al. Chemistry and clouds of Jupiter's atmosphere: a Galileo perspective. In: The three Galileos: the man, the spacecraft, the telescope; 1997. p. 249–60. doi:10.1007/978-94-015-8790-7_21.
[9] Atreya SK, et al. Comparison of the atmospheres of Jupiter and Saturn: deep atmospheric composition, cloud structure, vertical mixing, and origin. Planet Space Sci 1999;47:1243–62. doi:10.1016/S0032-0633(99)00047-1.
[10] Drossart P, et al. The solar reflected component in Jupiter's 5-μm spectra from NIMS/Galileo observations. J Geophys Res 1998;103(E10):23043–9. doi:10.1029/98JE01899.
[11] Irwin PGJ, et al. The origin of belt/zone contrasts in the atmosphere of jupiter and their correlation with 5-μm opacity. Icarus 2001;149:397–415. doi:10.1006/icar.2000.6542.
[12] Sindoni G, et al. Characterization of the white ovals on Jupiter's southern hemisphere using the first data by the Juno/JIRAM instrument. Geophys Res Lett 2017;44. doi:10.1002/2017GL072940.
[13] Grassi D, et al. The Venus nighttime atmosphere as observed by the VIRTIS-M instrument. Average fields from the complete infrared data set. J Geophys Res Planets 2014;119:837–49. doi:10.1002/2013JE004586.
[14] Stamnes K, et al. Numerically stable algorithm for discrete-ordinate-method radiative transfer in multiple scattering and emitting layered media. Appl Opt 1998;27(12):2502–9.
[15] Irwin PGJ, et al. The NEMESIS planetary atmosphere radiative transfer and retrieval tool. J Quant Spectrosc Radiat Transf 2007;109:1136–50. doi:10.1016/j.jqsrt.2007.11.006.
[16] Irwin PGJ, et al. Calculated k distribution coefficients for hydrogen- and self-broadened methane in the range 2000–9500 cm−1 from exponential sum fitting to band-modelled spectra. J Geophys Res 1996;101(E11):26137–54. doi:10.1029/96JE02707.
[17] Rothman LS, et al. The HITRAN2012 molecular spectroscopic database. J Quant Spectrosc Radiat 2013;130:4–50. doi:10.1016/j.jqsrt.2013.07.002.
[18] Kylling A, et al. A reliable and efficient two-stream algorithm for spherical radiative transfer: documentation of accuracy in realistic layered media. J Atmos Chem 1995;21:115–50. doi:10.1007/BF00696577.
[19] Seiff A, et al. Thermal structure of Jupiter's atmosphere near the edge of a 5-μm hot spot in the north equatorial belt. J Geophys Res 1998;103(E10):22857–89 Available as numerical data as GP-J-ASI-3-ENTRY-V1.0, NASA Planetary Data System. doi:10.1029/98JE01766.

[20] Tran H, et al. Model, software, and database for line-mixing effects in the $\nu 3$ and $\nu 4$ bands of CH4 and tests using laboratory and planetary measurements. H2 (and He) broadening and the atmospheres of Jupiter and Saturn. J Quant Spectrosc Radiat Tranf 2006;101:306–24. doi:10.1016/j.jqsrt.2005.11.020.
[21] Devi MalathyV, et al. Line positions and intensities of the phosphine (PH3) Pentad near 4.5 µm. J Mol Spect 2014;289:11–23. doi:10.1016/j.jms.2014.01.013.
[22] Devi MalathyV, et al. Line shape parameters of PH3 transitions in the Pentad near 4–5 µm: Self-broadened widths, shifts, line mixing and speed dependence. J Mol Spect 2014;302:17–33. doi:10.1016/j.jms.2014.06.003.
[23] Giles RS, et al. Cloud structure and composition of Jupiter's troposphere from 5-m Cassini VIMS spectroscopy. Icarus 2015;257:457–70. doi:10.1016/j.icarus.2015.05.030.
[24] Ragent B, et al. The clouds of Jupiter: results of the Galileo Jupiter mission probe nephelometer experiment. J Geophys Res 1998;103(E10):22891–909. doi:10.1029/98JE00353.
[25] Press WH, et al. Numerical recipes in Fortran 90: the art of parallel scientific computing. Cambridge University Press; 1996.
[26] Nixon CA. Atmospheric composition and cloud structure in Jovian 5-µm hotspots from analysis of Galileo NIMS measurements. Icarus 2001;150:48–68. doi:10.1006/icar.2000.6561.
[27] Giles RS, et al. Latitudinal variability in Jupiter's tropospheric disequilibrium species: $GeH_4$, $AsH_3$ and $PH_3$, accepted for publication. Icarus 2016;1610:09073 arXiv.
[28] Grassi D, et al. Preliminary results on the composition of Jupiter's troposphere in hot spots regions from the JIRAM/Juno instrument. Geophys Res Lett 2017;44. doi:10.1002/2017GL072841.
[29] Mlawer EJ, et al. Development and recent evaluation of the MT_CKD model of continuum absorption. Philos Trans R Soc London Ser A 2012;370:2520–56. doi:10.1098/rsta.2011.0295.
[30] Plass GN, Kattawar GW, Catchings FE. Matrix operator theory of radiative transfer. 1: Rayleigh scattering. Appl Opt 1973;12:314–29.
[31] Ignatiev NI, Grassi D, Zasova LV. Planetary Fourier spectrometer data analysis: fast radiative transfer models. Planet Space Sci 2005;53(10). doi:10.1016/j.pss.2004.12.009.